Water Air Soil Pollut (2024) 235:198
https://doi.org/10.1007/s11270-024-07000-z

Experimental Study on Evaluation of Pumpkin Waste in Removal of Textile Dyes: Preparation, Characterization, Adsorption, and Desorption

Oznur Dursun · Sahra Dandil · Caglayan Acikgoz

Received: 12 May 2023 / Accepted: 23 February 2024 / Published online: 6 March 2024

Abstract In this study, the use of natural waste containing the outer shell and seed shells of pumpkin (WSSP) in synthetic Reactive Blue 3R (RB) and Reactive Red P4BN (RR) dye removal processes was investigated. The chemical characterization of WSSP was presented by Fourier transform infrared spectroscopy (FTIR) analysis. Scanning electron microscopy (SEM) images showed the morphologies of the samples. Thermogravimetric analysis (TGA) and differential thermal analysis (DTA) curves were obtained to investigate the thermal behavior of the WSSP. Batch adsorption studies were carried out between pH 1–8, and the highest removals were obtained for RB and RR dyes as 66% at pH 3 and 92% at pH 1, respectively. The equilibrium was reached in 180 min for RB and 300 min for RR dye removal processes. The decreased particle size of the WSSP encouraged the adsorption rate. Adsorption kinetics of both processes fit pseudo-second-order kinetics. The equilibrium studies of the dye removal processes were best clarified by the Langmuir isotherm model. Enthalpy (ΔH^0) and entropy (ΔS^0) values of the RB dye adsorption process were 41.49 kJ mol^{-1} and 139.65 J $mol^{-1}K^{-1}$, respectively. For the RR dye removal process, ΔH^0 value was obtained as −38.94 kJ mol^{-1} and ΔS^0 value as −118.49 J $mol^{-1}K^{-1}$. Negative Gibb's free energy (ΔG^0) values were determined for both dyes. In desorption studies, the highest desorption percentage was determined for both dyes with pH 12 distilled water. It has been determined that WSSP provides effective dye removal as an alternative and a low-cost adsorbent.

Keywords Adsorbent · Isotherm · Kinetic · Pollutant · Thermodynamic

1 Introduction

Pollutants due to industrial activities mixed with water lead to a serious hazard for both the environment and living. Wastewater containing pollutants released from the chemical industry is extremely dangerous; however, they are not biodegradable (Wasewar et al., 2020). One of the well-known of these pollutants is dyes. Because of their intense utility in industry, they are frequently encountered in industrial wastewater (Roy & Saha, 2021). Reactive dyes are water-soluble anionic dyes that stand out due to their bright colors, fastness properties, and easy application (Chattopadhyay, 2011; Gopalakrishnan et al., 2019). Fastness properties are a result of the presence of strong dye-fiber interaction due to the formation of covalent bonds with fiber (Chakraborty, 2010). Nevertheless, they can mix with water due to the frequent use of reactive dyes or their low fixation with

O. Dursun · S. Dandil · C. Acikgoz (✉)
Department of Chemical Engineering, Faculty of Engineering, Bilecik Seyh Edebali University, Bilecik, Türkiye
e-mail: caglayan.acikgoz@bilecik.edu.tr

some substrates (Li et al., 2024). In addition to negatively affecting aquatic life when they mix with water, they can cause health problems such as skin and respiratory problems, allergies, and even cancer (Singh et al., 2024). Thus, it is very important to remove them from water, and many studies are being carried out for this purpose. Among the reactive dyes, Reactive Red P4BN (RR) dye is used for dyeing cellulose fibers (cotton and viscose), while Reactive Blue 3R (RB) is used for textile dyeing and printing (indiamart, 2024).

Especially in recent years, due to the concern of not being able to reach clean water resources in the world, most of the attention is directed to the cleaning of pollutants such as dyes in wastewater and making the water reusable. Various methods like ion exchange, biological treatment, membrane filtration, oxidation, and adsorption are used to remove different types of dyes (Ahmad et al., 2015). The adsorption method is a commonly used and intensively examined and enhanced topic on the pollutant removal. The applicability of the adsorption processes is cheap, easily controllable, reproducible, and reusable adsorbents are the remarkable advantages of the method (Yin et al., 2023). Although adsorbents used to remove pollutants in adsorption processes can be natural or synthetic materials, the issue that researchers have given importance to in order not to restrict these superior properties of adsorption processes is to obtain environmentally harmless and low-cost adsorbents (Shunda et al., 2023). Instead of synthetic adsorbents, the evaluation of natural materials that do not require high costs to synthesize, are easily available, and contribute to the recycling of environmental waste is a very valuable issue. High removal ratios can be achieved by optimizing the variables of the adsorption process where natural waste materials are to be used, depending on the pollution factor desired to be removed (Mahmoodi et al., 2010; Senthilkumaar et al., 2006; Sulak et al., 2007; Witek-Krowiak et al., 2011; Yu et al., 2000).

There are some studies in the literature on adsorbents obtained from pumpkin shells or seed shells of pumpkin as a natural waste. In the studies, activated carbon obtained by carbonization of pumpkin waste was used as an adsorbent (Bal et al., 2021; Demiral & Şamdan, 2016; Hameed & El-Khaiary, 2008; Kowalkowska & Jóźwiak, 2019; Okoye et al., 2010; Rashid et al., 2019; Subbaiah & Kim, 2016). However, an adsorption study using the adsorbent obtained from the mixture of outer shell and seed shells of pumpkin was not found.

In this study, to evaluate all waste from a pumpkin, the waste containing the outer shell and seed shells of the pumpkin (WSSP) was examined as an economical adsorbent, and the development of an environmentally friendly process was studied by using this adsorbent without the need for any further treatment. The removal efficiency of WSSP was tested in the removal of RB and RR dyes. The parameters such as pH of RB and RR dye solutions, contact time for WSSP-RB dye and WSSP-RR dye, concentration of RB and RR dye solutions, amount and particle size of WSSP, and temperature of medium of the adsorption processes to remove RB and RR dyes from synthetic wastewater by WSSP were studied. Fourier transform infrared spectroscopy (FTIR) and scanning electron microscopy (SEM) analyzes for WSSP, at pH values which WSSP provided the highest removals, and WSSP before and after adsorption, and thermogravimetric analysis (TGA) for WSSP were performed. Kinetic studies of the processes were also examined. Isotherms were used to investigate the equilibrium states of the processes. The realization of the adsorptions was explained with thermodynamic studies performed depending on temperature. Additionally, desorption experiments were achieved with pH 8 distilled water, pH 10 distilled water, pH 12 distilled water, 0.2 M sodium hydroxide (NaOH), 1 M NaOH, and 0.1 M sodium carbonate (Na_2CO_3).

2 Materials and Methods

2.1 Materials and Preparation of WSSP

A pumpkin purchased from Bilecik market was washed, and then its outer shell was peeled, seeds were removed and seed shells were separated. The outer shells and seed shells, as the waste of the pumpkin, were dried in daylight for 15–20 days. The dried shells were ground by a grinder. The ground outer shells and seed shells of pumpkin were sieved, and different sized samples were obtained. The samples were obtained in four different size ranges as 0.090–0.250, 0.250–0.425, 0.425-0.600, and 0.600–0.850 mm, separately for both the outer shell

and the seed shells. These samples were mixed at a ratio of 1:1 by mass, and WSSP was prepared.

RB and RR dyes were obtained from a textile factory in Türkiye. The wavelengths at which both dyes reach maximum absorbance were determined by ultraviolet-visible (UV-Vis) spectrophotometer (PG Instruments T-80) and were found to be 585 nm and 535 nm for RB and RR, respectively. 0.1 M, 0.5 M, 1.0 M NaOH, and hydrochloric acid (HCl) solutions were used to adjust the pH values of the dye solutions.

2.2 Methods

2.2.1 Zero-Point Charge Determination

Zero-point charge determination experiments were performed similar to a previously published study (Bello et al., 2021). A 0.01 M sodium chloride (NaCl) solution was prepared, and 50 mL of each was placed in 13 glass flasks. Their pH values were adjusted in the range of 1–13. 0.2 g of 0.090–0.250 mm sized WSSP was added to each prepared solution. The solutions were placed in a shaker (Memmert, WNB 22) at room temperature at a shaking speed of 120 rpm. After 24 h, the final pHs were measured. ΔpHs were calculated by subtracting the initial pH values (pHi) from the final measured pH values. Then, pHi versus ΔpH was plotted.

2.2.2 Adsorption Studies

Experiments of RB and RR removal with WSSP were achieved with synthetically prepared 50 mL dye solutions. Experiments were performed in a shaking water bath at a constant shaking speed of 120 rpm. It was found that when WSSP was added to water, it gave a distinctive color and therefore the color of the medium changed. To prevent this, blank samples were used in all steps of the experiments. Adsorption parameters were determined as pH (1–8), time (0–24 h), initial dye concentration (20–100 ppm), amount of adsorbent (0.05–0.5 g), adsorbent particle size (0.090–0.850 mm), and temperature (25–45 °C) and investigated by batch experiments. For determining the dye concentrations in the aqueous solutions, 6 mL samples were taken each time and centrifuged for 3 min at 3000 rpm. After centrifugation, absorbances were determined by the UV-Vis spectrophotometer.

2.2.3 Desorption Studies

The desorption performance of the RB and RR dye adsorption processes using WSSP was examined. Desorption studies, similar to previous studies, including first saturating WSSP with the dyes and then examining its performance in different desorbing environments (Bhatti et al., 2020; Ip et al., 2009; Li et al., 2009; Purkait et al., 2005). Adsorptions were carried out for RB and RR dye at pH 3 and pH 1, respectively, at 2000 ppm dye concentration, 0.5 g WSSP for 500 mL dye solution, 0.090–0.850 mm WSSP particle size, 120 rpm, and room temperature conditions until equilibrium time. The dilution process was applied for UV-Vis spectrophotometer readings of the samples. Then, desorption experiments were carried out for 0.05 g/50 mL at 120 rpm and room temperature. The effectiveness of pH 8 distilled water, pH 10 distilled water, pH 12 distilled water, 0.2 M NaOH, 1 M NaOH, and 0.1 M Na_2CO_3 was tested for the desorption of RB and RR dyes.

2.3 FTIR, SEM, and TGA Analysis

Characterization of functional groups for WSSP, WSSP in acidic environments and WSSP before and after adsorption was analyzed by FTIR spectrometer (Perkin Elmer LR64912C). Analyzes of the samples were performed between 4000 and 400 cm^{-1}. ZEISS Supra 40 VP brand SEM device was used to determine the morphological features. The morphological structures of WSSP, WSSP in pH 1 aqueous solution, WSSP in pH 3 aqueous solution, and WSSP after adsorption were determined. The thermal behavior of WSSP was investigated with a TG/DTA device (EXSTAR SII TGA/DTA 7200). TGA and differential thermal analysis (DTA) were performed by heating at a rate of 10°C/min in the range of 30–800°C in a nitrogen atmosphere.

2.4 Evaluation of Data

The adsorption capacities and the removal percentage values were calculated with the following equations (Sultana et al., 2022):

$$q_e = \frac{(C_0 - C_e)xV}{m} \quad (1)$$

$$\text{removal efficiency} = \frac{(C_0 - C_e)x100}{C_0} \quad (2)$$

where q_e represents the dye amount in equilibrium on the adsorbent (mg g^{-1}), C_o represents the initial dye concentration (mg L^{-1}), C_e represents the dye concentration in the equilibrium (mg L^{-1}), V represents the volume of the solution (L), and m represents the mass of the adsorbent (g) (Sultana et al., 2022).

To examine the kinetics of the adsorption processes, pseudo-first-order, pseudo-second-order, and intra-particle diffusion models were studied. Equations of the kinetic models are given below (Debnath & Das, 2023; Zhang et al., 2023):

$$\text{Pseudo} - \text{first} - \text{order} : \log(\text{qe} - \text{qt}) = \log\text{qe} - \frac{k_1}{2.303}\text{t} \quad (3)$$

$$\text{Pseudo} - \text{second} - \text{order} : \frac{t}{q_t} = \frac{1}{k_2 q_e^2} + \frac{t}{q_e} \quad (4)$$

$$\text{Intra} - \text{particle diffusion} := k_{int} t^{0.5} + \text{C} \quad (5)$$

where t is time (min), q_t represents the amount of adsorbate adsorbed on the adsorbent at time t (mg g^{-1}), k_1 represents the pseudo-first-order rate constant (min^{-1}), k_2 represents the second-order rate constant (g mg^{-1} min^{-1}), k_{int} represents the intraparticle diffusion rate constant (mg g^{-1} $min^{-0.5}$), and C represents a constant (Debnath & Das, 2023; Zhang et al., 2023).

Langmuir and Freundlich isotherm equations used for equilibrium studies of adsorption processes are as follows (Gad et al., 2023):

$$\text{Langmuir isotherm} : \frac{C_e}{q_e} = \frac{C_e}{q_m} + \frac{1}{(q_m K_L)} \quad (6)$$

$$\text{Freundlich isotherm} : \ln q_e = \ln K_F + \frac{1}{n} \ln C_e \quad (7)$$

where K_L represents the Langmuir isotherm constant (L g^{-1}), q_m represents the maximum adsorption capacity (mg g^{-1}), K_F represents the Freundlich isotherm constant ((mg g^{-1} (L $mg^{-1})^{1/n}$)), and n represents the linearity constant for Freundlich (Gad et al., 2023).

The equations used to determine the thermodynamic parameters are listed below (Alalwan et al., 2021):

$$\ln K_d = -\frac{\Delta H^0}{RT} + \frac{\Delta S^0}{R} \quad (8)$$

$$K_d = \frac{q_e}{C_e} \quad (9)$$

$$\Delta G^0 = \Delta H^0 - T\Delta S^0 \quad (10)$$

where ΔH^0 represents the enthalpy (kJ mol^{-1}), ΔS^0 represents the entropy (J $mol^{-1}K^{-1}$), ΔG^0 represents Gibb's free energy (kJ mol^{-1}), T represents the temperature (K), K_d represents the adsorption equilibrium constant, and R represents the gas constant (8.314 J mol^{-1} K^{-1}) (Alalwan et al., 2021).

3 Results and Discussion

3.1 Results of FTIR, SEM, and TGA Analysis

3.1.1 FTIR Analysis

FTIR spectroscopy was used to chemically analyze the adsorbent, determine the changes in the chemical structure of the adsorbent by the acidic environment (pH 1 and pH 3, where the best removals are obtained), and chemically characterize it after adsorption. FTIR analyzes are shown for WSSP, WSSP in aqueous solution at pH 1 (WSSP-pH 1), WSSP in aqueous solution at pH 3 (WSSP-pH 3), after adsorption of RB dye (WSSP+RB), and after adsorption of RR dye (WSSP+RR) in Fig. 1a.

The wide absorption bands in the range of 3296.80–3331.47 cm^{-1} observed for WSSP and other samples were interpreted as the presence of hydrogen-bonded O-H groups (Müller et al., 2011; Schramm, 2020). The bands around 2920.21–2921.36 and 2850.66–2852.36 cm^{-1} may show the C–H groups (Qin et al., 2010; Wen et al., 2014). The peaks around 2160 may belong to C-N (Hadjiivanov et al., 2020). The peaks around 2030 may indicate CO groups (Mihaylov et al., 2011). Strong bands that may be attributed to C=C vibrations in the structure of the samples are seen around 1636.97–1650.64 cm^{-1} (Pazo-Cepeda et al., 2023; Strauss et al., 2020). While the -CONH- peak seen at 1544 cm^{-1} for WSSP was also evident for WSSP+RR, which may be due to the structure of the RR dye, it lost its effect for the other

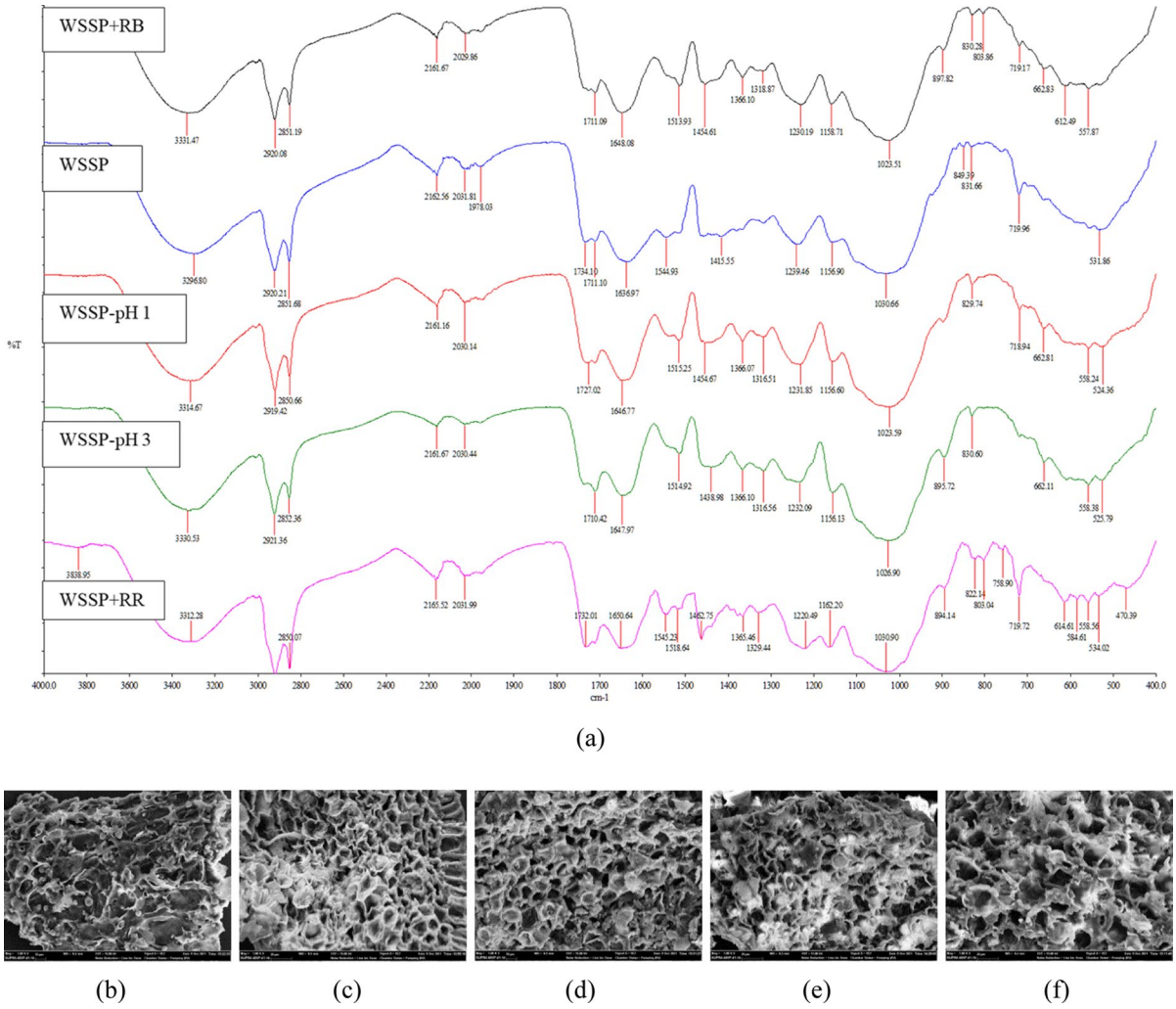

Fig. 1 **a** FTIR spectra, SEM images of **b** WSSP, **c** WSSP-pH 1, **d** WSSP-pH 3, **e** WSSP+RB, **f** WSSP+RR, and **g** TG/DTA curves of WSSP in the nitrogen atmosphere

samples and strengthened a peak by shifting between 1513–1519 cm^{-1} for all samples except WSSP (Gaikwad & Mukherjee, 2021; Kazemi et al., 2023). The 1365–1367 cm^{-1} peaks, which are not seen for WSSP and belong to the C-O interaction, were seen in both acidic and after dye adsorption samples and may indicate that they are the groups that provide adsorption (Moradzaman & Mul, 2020). Bands in the range of 1300–900 cm^{-1} are generally for C–O stretching vibration and C-H bends (Vunain et al., 2017). The 894–898 cm^{-1} peaks, which are not evident for WSSP and provide adsorption by C-H interaction, became evident in other samples (Gonultas & Candan, 2018). For WSSP+RB and WSSP+RR, peaks indicating adsorption via C-H bonds appeared in the range of 803–804 cm^{-1} (Zimmerman et al., 1999). Absorption bands in the 700–470 cm^{-1} region may indicate the presence of sulfur especially in WSSP+RB and WSSP+RR due to the chemical structure of the dyes (Wang et al., 1998).

3.1.2 SEM Analysis

SEM analyzes were performed for WSSP, WSSP-pH 1, WSSP-pH 3, WSSP+RB, and WSSP+RR. In the SEM image of WSSP shown in Fig. 1b, it was observed that there were irregular structures on the surface of the adsorbent in the form of holes

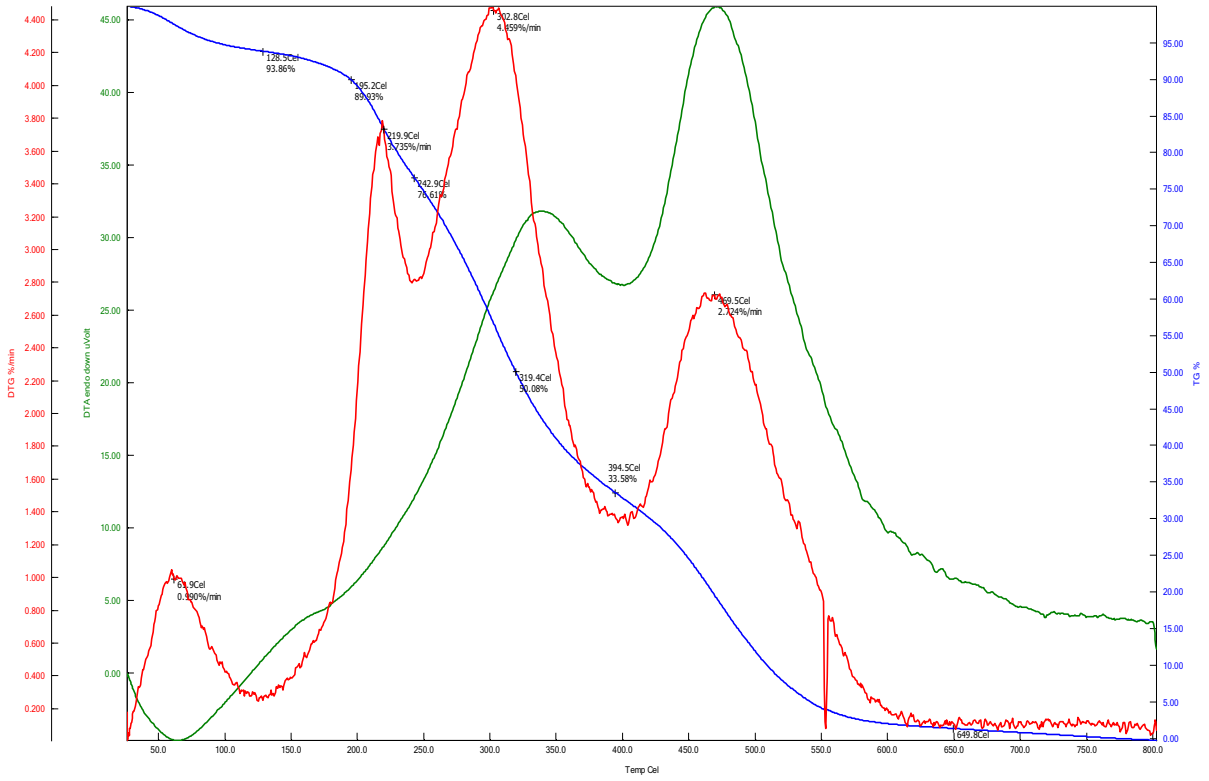

(g)

Fig. 1 (continued)

and round particles of different shapes, which are thought to be caused by the use of the outer shells of the pumpkin and its seeds. In Fig. 1c for WSSP-pH 1, it has been that there were no round-shaped particles and uniform and more regular pores were formed in the structure. In Fig. 1d, it is seen that the pores of WSSP-pH 3 are more open, smooth, and distinct. It was interpreted that the formation of these porous and regular structures of WSSP-pH 1 and WSSP-pH 3 forms the basis for the dye adsorptions. Fig. 1e and f are SEM images of RB and RR dyes after adsorption on WSSP, respectively. According to these figures, it is seen that the dye molecules hold onto the pores of WSSP and fill the pores. However, it was also determined that the adsorbent offers more capacity for dye adsorption since the pores are not completely filled.

3.1.3 TGA Analysis

The TG and DTA curves of WSSP are shown in Fig. 1g. The removal of adsorbed water in the sample occurred in the range of 30–128 °C. It is observed that 6.14 % mass loss occurs in the sample with the removal of water. The TG curve showed that the sample disintegrated in three steps. The first disintegration step may cause the low molecular weight constituents to correspond to a mass loss of 17.25 % in the range of 128–243 °C (Xu et al., 2020). There is a 43.02 % mass loss in the range of 243–394 °C, where the second disintegration step is observed. The second step may have been caused by hemicellulose disintegration (Rawat & Ahammed, 2023). 33.58 % mass loss was determined in the last disintegration step, which took place between 394 and 650

°C may be due to the disintegration of cellulose and lignin (Atalay et al., 2022). The maximum degradation rates of the degradation steps are 3.73, 4.46, and 2.72 %/min, respectively. The disintegration process, which takes place in three steps, proves that groups of different molecular weights are removed from the sample structure. An endothermic transition with a maximum of 62 °C was observed in the DTA curve of the sample, indicating the removal of adsorbed water. In addition, exothermic transitions showing the oxidation (combustion) of the sample in the DTA curve were observed at 340°C and 470°C.

3.2 Dye Solution pH and Contact Time

Dye solution pH and contact time experiments were performed simultaneously for 50 mg/L, 0.090–0.250 mm particle size, 0.05 g WSSP, and 25°C. The

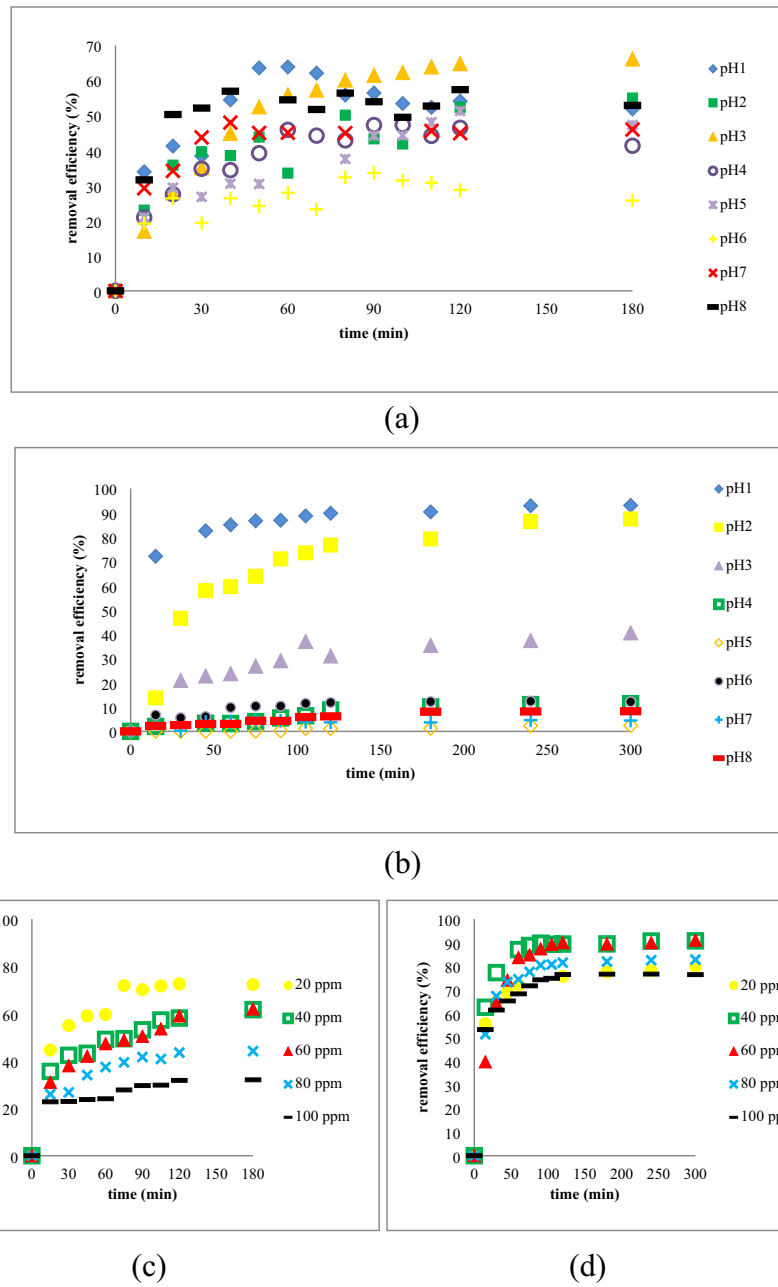

Fig. 2 pH effect on the removal of **a** RB and **b** RR over time, effect of initial dye concentration on the adsorption of **c** RB and **d** RR dyes on WSSP, effect of adsorbent amount on **e** RB and **f** RR dye adsorption on WSSP, contact time–adsorption capacity graph of **g** RB and **h** RR dyes for adsorption on WSSP, effect of particle size of WSSP on **i** RB and **j** RR dye removal

Fig. 2 (continued)

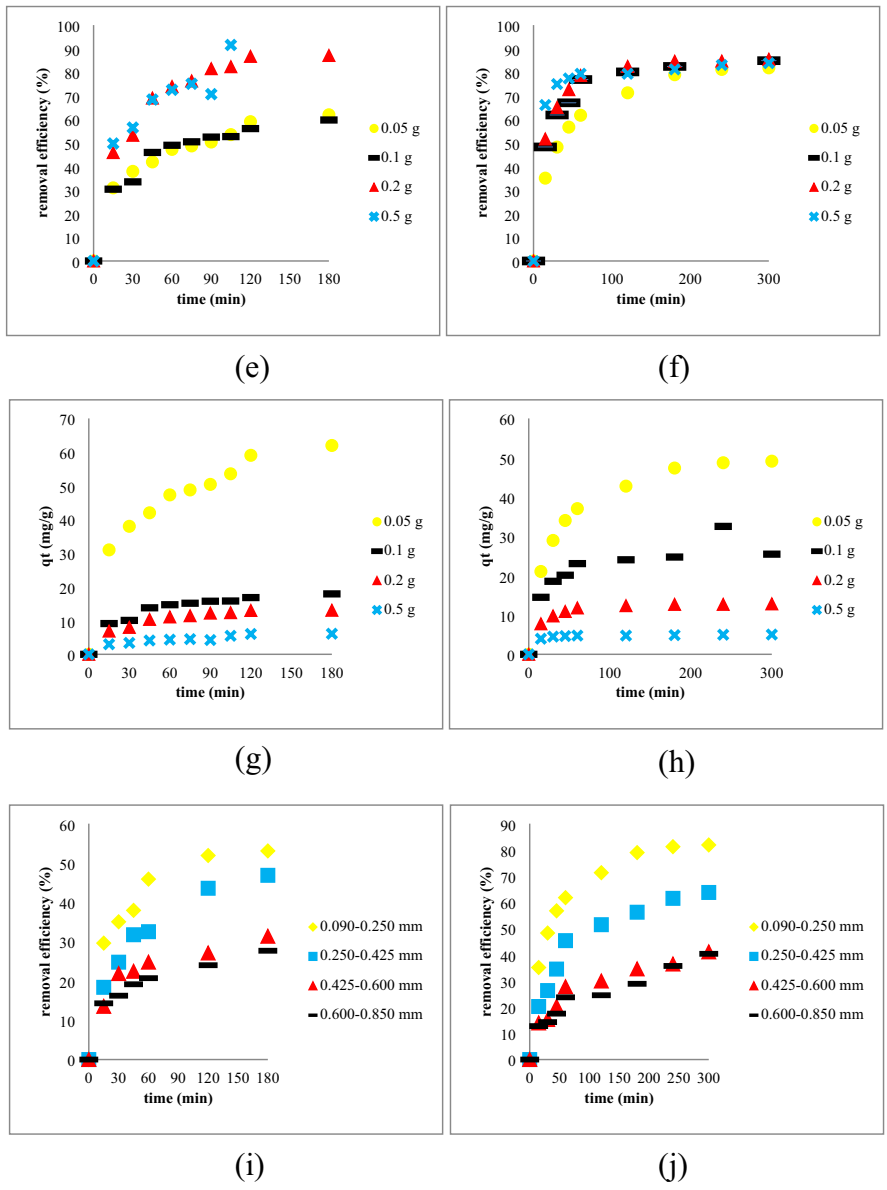

removal efficiencies over time depending on the initial pH values of the RB and RR removal processes using WSSP are exhibited in Fig. 2a and b, respectively. According to Fig. 2a and b which belong to the adsorption of RB and RR, respectively; the removal values for each pH value increased with time until the equilibrium time were reached. The equilibrium time for RB and RR removal processes was determined as 180 and 300 min, respectively.

In Fig. 2a and b, it is seen that the removals are higher at low pH values at equilibrium times for both dyes. According to this; while the maximum removal percentage for RB dye was 66% at pH 3, it was 92% at pH 1 for RR. Thus, subsequent experiments were carried out at pH 3 and 1 for RB for RR, respectively, where the highest removals were obtained. Since the hydroxyl (H^+) ion concentration in the solution increases at low pH, the surface of WSSP is charged positively. Because of the anionic character of reactive RB and RR dyes, the dye molecules and WSSP interact strongly. Therefore, the percentage of adsorption is higher at low pH values (Kumar et al., 2010). The fact that dyes provide maximum removal at different pH values can be explained as the different

groups and atoms they contain, depending on the different structures of the dyes, affect their interaction with WSSP (Ahamad & Nasar, 2024; Arunkumar et al., 2024). In addition, the zero-point charge of WSSP was obtained as 5.9. The zero-point charge of a solution describes that the density of cations is equal to that of anions on the surface (Ducheyne, 2015). Thus, in cases where the pH of the solution is lower than the zero-point charge of WSSP, which is determined as 5.9, the surface of WSSP charges positively and strongly adsorbs the anionic RB and RR dyes (Wang et al., 2024).

3.3 Dye Concentration

To determine the effect of the initial dye concentrations on the adsorption efficiency, the time-dependent changes in removal efficiencies of the dyes at the determined concentrations were investigated and presented in Fig. 2c and d. Experimental conditions were 0.090–0.250 mm particle size, 0.05 g WSSP, and 25°C. As seen in Fig. 2c, the removal decreased as the initial concentration of RB increased. While the removal percentage values were 72% at 20 ppm, it was 32% at 100 ppm. In Fig. 2d, for the removal of RR dye, removal efficiencies were obtained as 80, 90, 91, 82, and 76 % for 20, 40, 60, 80, and 100 ppm, respectively. In this way, it was determined that the removal percentages increased up to 80 ppm for RR dye and then decreased. Similar to some studies in the literature, it was determined that different removal efficiencies were obtained for both dyes at different initial concentrations, depending on the adsorbing capacity of the WSSP and the structure of the RB and RR (Aragaw & Alene, 2022).

3.4 Adsorbent Amount

The studies of the amount of WSSP were carried out with four different amounts as 0.05, 0.1, 0.2, and 0.5 g. Other parameters were determined as 60 mg/L, 0.090–0.250 mm particle size, and 25 °C. The effect of the WSSP amount on the removal of the dyes using WSSP depending on the time is given in Fig. 2e–h. According to Fig. 2e and f, with an increase in the amount of WSSP from 0.05 g to 0.5 g, the removal of RB dye increased, but there was no significant increase in RR dye removal. Since the increase in the amount of WSSP increased the adsorbing sites for the adsorption of RB, the removal percentage was 62% when the amount of WSSP was 0.05 g and approached 100% when 0.5 g (Algethami et al., 2024). However, increasing the amount of WSSP did not increase the removal of RR dye because adsorption had already occurred for 0.05 g (Aljeboree et al., 2015).

In Fig. 2g and h, it is seen that the adsorption capacities for the adsorption of RB and RR dyes adsorbed on WSSP decreased by increasing the amount of WSSP from 0.05 to 0.5 g. From 0.05 to 0.5 g, the amount of dye retained per g adsorbent in the adsorption of RB decreased from 61.98 to 6.11 mg (Fig. 2g), in the removal of RR changed from 49.76 to 5.03 mg (Fig. 2h). The reason for this may be the unsaturation of the adsorbent active sites, which increases due to the increasing amount of adsorbent, or the amount of dye molecules against the active sites is quite insufficient in the high amount of adsorbent (El Kassimi et al., 2023).

3.5 Adsorbent Particle Size

For particle size effect determination experiments, conditions were settled as 60 mg/L, 0.05 g WSSP, 50 mL solution volume, 120 rpm, and 25 °C. The particle size effect of WSSP on the removal of RB and RR are shown in Fig. 2i and j, respectively. As shown in Fig. 2i and j, the decrease in particle size from >0.600 mm to 0.090–0.250 mm encouraged the removal efficiency for both dyes. Thus, the highest removals were obtained for particle size of adsorbent 0.090–0.250 mm for both dyes. The decrease in the particle size of WSSP caused an increase in the adsorptive sites required for the adsorbing of the dye molecules (Akpomie et al., 2017).

3.6 Adsorption Kinetic Studies

The pseudo-first-order, pseudo-second-order, and intraparticle diffusion kinetic models were performed to determine the behavior of the removal of RB and RR dyes using WSSP are given in Fig. 3a–f. In addition, the parameters of the kinetic models are given in Table 1. According to the correlation coefficient (R^2) of the kinetic models given in the table for the RB and RR removal, the pseudo-second-order kinetic model presented the highest value for both dyes and therefore the adsorptions followed the

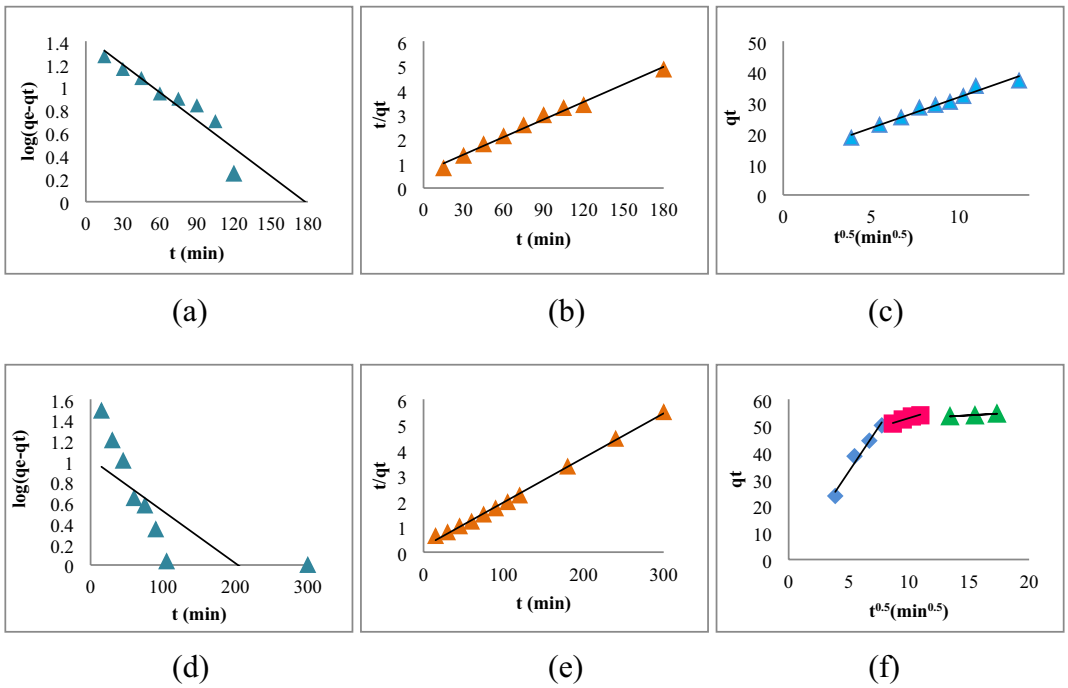

Fig. 3 Plots of the **a** pseudo-first-order, **b** pseudo-second-order, and **c** intraparticle diffusion kinetic models for the RB removal process, plots of the **d** pseudo-first-order, **e** pseudo-second-order, and **f** intraparticle diffusion kinetic models for the RR removal process, plots of the **g** Langmuir and **h** Freundlich isotherm models for the RB removal process, plots of the **i** Langmuir and **j** Freundlich isotherm models for the RR removal process, and Van't Hoff plots for adsorption of **k** RB and **l** RR dyes on WSSP

second-order kinetics. It is also seen that the experimental qe ($q_{e,exp}$) values for both dyes are close to the calculated qe ($q_{e,cal}$) values of the second-order kinetics and thus they support the suitability to the pseudo-second-order kinetic model (Meskel et al., 2024). The pseudo-second-order kinetic model emphasizes that chemical adsorption is effective in the processes (Siraorarnroj et al., 2022). In addition, the high R^2 values are obtained for the intraparticle diffusion model studies of RB and RR removal processes, showing that intraparticle diffusion is effective in both processes. The straight line for the adsorption of RB dye, which does not pass through the origin, is a situation observed in slow-stirred bulk adsorption and expresses that the mass transfer limits the rate (Gandhi et al., 2016). However, the three linear parts of the intraparticle diffusion plot for the adsorption of RR indicate that the process can be explained in three steps. For each linear portion, a higher slope indicates a faster adsorption process (Huang et al., 2018). The first linear part represents the boundary diffusion, which can also be expressed as the outer surface adsorption, where the adsorbate spreads on the outer surface of the adsorbent, the second linear part represents the intraparticle diffusion of the adsorbent into the pores, and the last linear part represents the stage where the adsorbate is adsorbed into the pores of the adsorbent (Deng et al., 2013; Huang et al., 2018).

3.7 Adsorption Equilibrium Isotherms

Equilibrium studies of the RB and RR dye removal processes using WSSP were explained by Langmuir and Freundlich models. Ce/qe - Ce and lnqe - Ce plots of Langmuir and Freundlich isotherms are given in Fig. 3g–j. R^2 values of RB dye were found to be 0.9707 for Langmuir isotherm and 0.725 for Freundlich isotherm. R^2 values for RR dye were determined as 0.9911 for Langmuir isotherm and 0.8741 for Freundlich isotherm. According to the highest R^2 values, it was determined that the both processes followed the Langmuir isotherm model.

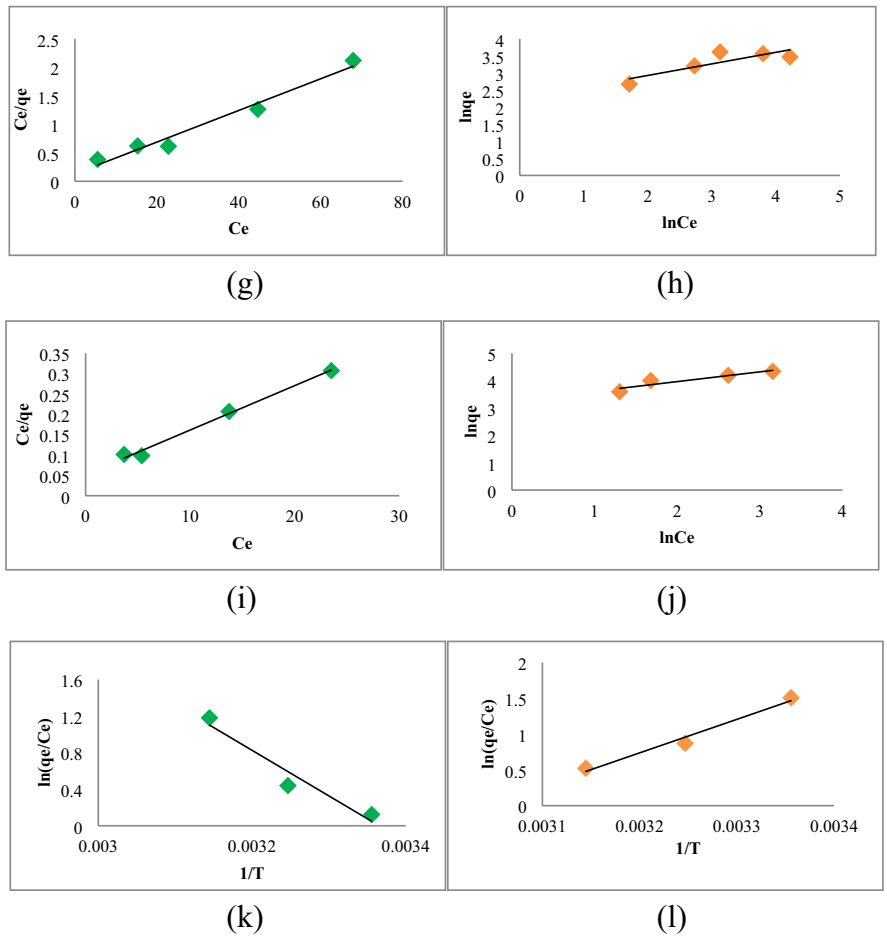

Fig. 3 (continued)

Table 2 shows the parameters of the equilibrium models. According to Table 2, q_m and K_L for the Langmuir model for RB adsorption were found to be 35.97 mg/g and 0.21 L/g, respectively. For RR adsorption, q_m and K_L values were calculated as 91.74 mg/g and 0.21 L/g, respectively. The Langmuir isotherm describes adsorption as monolayer and approves no interaction between the adsorbate molecules, and a high q_m value is expected to indicate a high surface area of WSSP (Martini et al., 2018).

3.8 Temperature and Thermodynamic

For RB dye, 53, 60, and 76% removal efficiencies and 32, 36, and 46 mg/g adsorption capacities were obtained for 25, 35, and 45°C, respectively. Thus, it was determined that the removal of RB dye increased with increasing temperature. For the removal of RR dye, removal efficiencies were obtained as 82, 70, and 63% and capacities were 49, 42, and 38 mg/g for 25, 35, and 45°C, respectively. RR removal decreased with increasing temperature.

Figure 3k and l show the Van't Hoff plots of the relationship of the adsorption equilibrium constant with temperature for the removal of RB and RR dyes using WSSP, respectively. The enthalpy (ΔH^0) and entropy (ΔS^0) values of the processes were obtained by using the slope ($-\Delta H^0/R$) and intercept ($\Delta S^0/R$) of the line in the graphs, respectively. According to the calculations, ΔH^0, ΔS^0, and Gibb's free energy (ΔG^0) values for the removal of RB and RR dyes on WSSP are given in Table 3. For the RB dye removal process using WSSP, ΔH^0 was calculated as 41.49 kJ mol^{-1}. The positive value of ΔH^0 explains the

Table 1 Kinetic parameters for adsorption of RB and RR dyes on WSSP

Kinetic model		RB	RR	
	$q_{e,\,exp}$	37.19	54.63	
Pseudo-first-order kinetic model	k_1 ($\times 10^3$)	18.65	11.52	
	$q_{e,\,cal}$	27.49	10.56	
	R^2	0.8757	0.6051	
Pseudo-second-order kinetic model	k_2 ($\times 10^3$)	0.88	1.48	
	$q_{e,cal}$	41.84	57.14	
	R^2	0.9888	0.9978	
Intra-particle diffusion model	R^2	0.9734	R^2_1	0.9736
			R^2_2	0.9614
			R^2_3	0.9521
	k_{int}	1.998	$k_{int,1}$	6.72
			$k_{int,2}$	1.38
			$k_{int,3}$	0.25
	C	11.81	C_1	−0.72
			C_2	39.16
			C_3	50.18

Table 2 Isotherm parameters for the adsorption of RB and RR dyes on WSSP

	Langmuir isotherm model			Freundlich isotherm model		
	K_L	q_m	R^2	K_F	n	R^2
RB	0.21	35.97	0.9707	9.49	2.95	0.725
RR	0.21	91.74	0.9911	25.83	2.81	0.8741

Table 3 Thermodynamic parameters for the adsorption of RB and RR dyes on WSSP

	T	ΔG^0	ΔH^0	ΔS^0
RB	298	−0.12	41.49	139.65
	308	−1.52		
	318	−2.91		
RR	298	−3.63	-38.94	-118.49
	308	−2.44		
	318	−1.26		

reaction to be endothermic (Khumalo et al., 2024). In an endothermic process, increasing temperature causes an increase in adsorption capacity (Al-Ghouti & Al-Absi, 2020). As given in the paragraph above, removal efficiency and adsorption capacity values were increased with increasing temperature for RB dye adsorption and supported the endothermicity of the process. ΔS^0 was found to be 139.65 J $mol^{-1}K^{-1}$, and this value defined the strong affinity of RB dye to WSSP on the surface and increased randomness at the interface (Chowdhury et al., 2011; Taqui et al., 2023). The positive values of $\Delta H°$ and $\Delta S°$ support that chemical adsorption is effective in the RB adsorption process on WSSP (Boughrara et al., 2022). For RR dye removal, ΔH^0 was found to be −38.94 kJ mol^{-1}. A negative ΔH^0 defines an exothermic process (Adjal et al., 2023). The fact that an adsorption process is exothermic means that the removal percentage and adsorption capacity of the process decreases due to the weakening interaction between the RR dye and WSSP with increasing temperature, supporting the behavior of the above RR adsorption process against temperature (Han et al., 2021). ΔS^0 was determined as −118.49 J $mol^{-1}K^{-1}$ and explained a more order state at the interface (Bassam et al., 2022). ΔG^0 refers to the process being spontaneous or non-spontaneous. A positive ΔG^0 indicates that the reaction cannot occur spontaneously and energy is needed for it to occur, while a negative ΔG^0 indicates spontaneity (Pepper, 2019). The ΔG^0 values of the adsorption processes for both dyes were calculated as negative for all temperatures studied, and therefore it was

stated that the adsorption took place spontaneously (Sadoq et al., 2024).

3.9 Desorption

Desorption studies were performed with pH 8 distilled water, pH 10 distilled water, pH 12 distilled water, 0.2 M NaOH, 1 M NaOH, and 0.1 M Na_2CO_3, and the desorption of RB and RR dyes from WSSP was determined. In the adsorptions performed at the beginning of the desorption studies, an adsorption percentage of 31% for RB dye and 70% for RR was determined. Figure 4a and b shows the desorption percentages of RB and RR dyes, respectively. As seen in Fig. 4a, desorption percentages of 3, 5, 14, 12, 11, and 12% for pH 8 distilled water, pH 10 distilled water, pH 12 distilled water, 0.2 M NaOH, 1 M NaOH, and 0.1 M Na_2CO_3, respectively, have been obtained for RB dye. Accordingly, the highest desorption was achieved with pH 12 distilled water, while the lowest was achieved with pH 8 distilled water for RB dye. In Fig. 4b of the desorption of RR, it is 3, 3, 7, 5, 4, and 5% for pH 8 distilled water, pH 10 distilled water, pH 12 distilled water, 0.2 M NaOH, 1 M NaOH, and 0.1 M Na_2CO_3, respectively, and the highest desorption was again achieved with pH 12 distilled water, while the lowest was achieved with pH 10 distilled water.

4 Comparative Study of Adsorption Capacity of WSSP with Other Similar Adsorbents

For the RB and RR removal processes using WSSP, the adsorption capacity of untreated WSSP used as an adsorbent was compared with the capacities of various other natural adsorbents, either treated or untreated, used in the literature and used for dye removal, and comparisons were given in Table 4. According to Table 4, the adsorption capacity of some untreated natural adsorbents can be high or low. Although it is known that the treatment

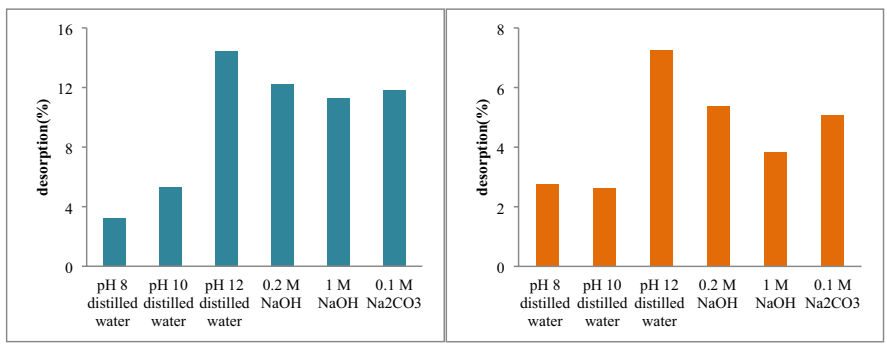

Fig. 4 Desorption percentages of **a** RB and **b** RR dyes

Table 4 Comparison of adsorption capacities of various natural adsorbents in dye removal

Adsorbent	q_{max}	Reference
Peanut hull	87.72	Gong et al. (2005)
Pomegranate peel	30.47	Ghibate et al. (2021)
Banana peel	211.9	Stavrinou et al. (2018)
Walnut shells powder	178.9	Miyah et al. (2018)
WSSP	91.74	Present study
Cationic surfactant-modified peanut husk	146.2	Zhao et al. (2017)
Pomegranate fruit peel activated carbon	250	Ahmad et al. (2021)
Fe-modified banana peel	28.1	Çatlıoğlu et al. (2021)
Amino functionalized walnut shells	224.4	Dovi et al. (2021)
Aminated pumpkin seed powder	200.3	Subbaiah and Kim (2016)

of adsorbents generally increases the adsorption capacity, some treated adsorbents may have low adsorption capacity.

5 Conclusions

In this study, the evaluation of WSSP in the removal of RB and RR dyes was examined. Characteristics of WSSP and process parameters were investigated. The surface morphologies and chemical characterizations of WSSP were determined by SEM and FTIR analyzes, respectively. The highest removal percentages were achieved at pH 3 and 1 for RB and RR, respectively. The adsorption process reached equilibrium at 180 min and 300 min for RB and RR, respectively. For both dyes, the highest adsorption capacities were reached at 0.05 g of WSSP. As WSSP particle sizes decreased, the removal percentages increased. Kinetics of the RB and RR dye removal processes followed the pseudo-second-order and intra-particle models. The Langmuir isotherm clarified the equilibrium state of both processes and thus proved the monolayer settlement of the dye molecules. While positive ΔH^0 and ΔS^0 values were obtained for the RB removal process, the RR process exhibited these values as negative. For both processes, ΔG^0 values explained that the processes occurred spontaneously. In desorption studies, the highest desorption percentage was determined for both dyes with pH 12 distilled water. This study represented that the RB and RR removal was successfully achieved using WSSP.

Author Contribution Conceptualization: Caglayan Acikgoz, Sahra Dandil, Oznur Dursun. Methodology: Caglayan Acikgoz, Sahra Dandil. Formal analysis and investigation: Caglayan Acikgoz, Sahra Dandil. Writing—original draft preparation: Caglayan Acikgoz, Sahra Dandil. Writing—review and editing: Caglayan Acikgoz, Sahra Dandil, Oznur Dursun. Supervision: Caglayan Acikgoz, Sahra Dandil

Data Availability All data generated or analyzed during this study are included in this published article.

Declarations

Ethical Approval Not applicable

Competing Interests The authors declare no competing interests.

References

Adjal, C., Timón, V., Guechtouli, N., Boussassi, R., Hammoutène, D., & Senent, M. L. (2023). The role of water in the adsorption of nitro-organic pollutants on activated carbon. *The Journal of Physical Chemistry A, 127*(39), 8146–8158. https://doi.org/10.1021/acs.jpca.3c03877

Ahamad, Z., & Nasar, A. (2024). Polypyrrole-decorated bentonite magnetic nanocomposite: A green approach for adsorption of anionic methyl orange and cationic crystal violet dyes from contaminated water. *Environmental Research, 247*, 118193. https://doi.org/10.1016/j.envres.2024.118193

Ahmad, A., Mohd-Setapar, S. H., Chuong, C. S., Khatoon, A., Wani, W. A., Kumar, R., & Rafatullah, M. (2015). Recent advances in new generation dye removal technologies: Novel search for approaches to reprocess wastewater. *RSC Advances, 5*(39), 30801–30818. https://doi.org/10.1039/C4RA16959J

Ahmad, M. A., Eusoff, M. A., Oladoye, P. O., Adegoke, K. A., & Bello, O. S. (2021). Optimization and batch studies on adsorption of methylene blue dye using pomegranate fruit peel based adsorbent. *Chemical Data Collections, 32*, 100676. https://doi.org/10.1016/j.cdc.2021.100676

Akpomie, K., Onoabedje, E., Alumona, T., Alum, O., Okagu, O., & Ezeofor, C. (2017). Attenuation of methylene blue from aqua-media on acid activated montmorillonite of Nigerian origin. *Journal of Environmental Science and Management, 20*(2). https://doi.org/10.47125/jesam/2017_2/03

Alalwan, H. A., Mohammed, M. M., Sultan, A. J., Abbas, M. N., Ibrahim, T. A., Aljaafari, H. A., & Alminshid, A. A. (2021). Adsorption of methyl green stain from aqueous solutions using non-conventional adsorbent media: Isothermal kinetic and thermodynamic studies. *Bioresource Technology Reports, 14*, 100680. https://doi.org/10.1016/j.biteb.2021.100680

Algethami, J. S., Alhamami, M. A., Alqadami, A. A., Melhi, S., & Seliem, A. F. (2024). Magnetic hydrochar grafted-chitosan for enhanced efficient adsorption of malachite green dye from aqueous solutions: Modeling, adsorption behavior, and mechanism analysis. *International Journal of Biological Macromolecules, 254*, 127767. https://doi.org/10.1016/j.ijbiomac.2023.127767

Al-Ghouti, M. A., & Al-Absi, R. S. (2020). Mechanistic understanding of the adsorption and thermodynamic aspects of cationic methylene blue dye onto cellulosic olive stones biomass from wastewater. *Scientific Reports, 10*(1), 15928. https://doi.org/10.1038/s41598-020-72996-3

Aljeboree, A. M., Alkaim, A. F., & Al-Dujaili, A. H. (2015). Adsorption isotherm, kinetic modeling and thermodynamics of crystal violet dye on coconut husk-based activated carbon. *Desalination and Water Treatment, 53*(13), 3656–3667. https://doi.org/10.1080/19443994.2013.877854

Aragaw, T. A., & Alene, A. N. (2022). A comparative study of acidic, basic, and reactive dyes adsorption from aqueous solution onto kaolin adsorbent: Effect of operating parameters, isotherms, kinetics, and thermodynamics. *Emerging Contaminants, 8*, 59–74. https://doi.org/10.1016/j.emcon.2022.01.002

Arunkumar, G., Deviga, G., Mariappan, M., Pannipara, M., Al-Sehemi, A. G., & Anthony, S. P. (2024). Natural tea extract coated porous MOF nano/microparticles for highly enhanced and selective adsorption of cationic dyes from aqueous medium. *Journal of Molecular Liquids, 394*, 123747. https://doi.org/10.1016/j.molliq.2023.123747

Atalay, S., Sargin, I., & Arslan, G. (2022). Crystallization of struvite-K from pumpkin wastes. *Journal of the Science of Food and Agriculture, 102*(2), 523–530. https://doi.org/10.1002/jsfa.11380

Bal, D., Özer, Ç., & İmamoğlu, M. (2021). Green and ecofriendly biochar preparation from pumpkin peel and its usage as an adsorbent for methylene blue removal from aqueous solutions. *Water, Air, & Soil Pollution, 232*(11), 1–16. https://doi.org/10.1007/s11270-021-05411-w

Bassam, R., El Alouani, M., Maissara, J., Jarmouni, N., Belhabra, M., Chbihi, M. E. M., & Belaaouad, S. (2022). Investigation of competitive adsorption and desorption of heavy metals from aqueous solution using raw rock: Characterization kinetic, isotherm, and thermodynamic. *Materials Today: Proceedings, 52*, 158–165. https://doi.org/10.1016/j.matpr.2021.11.450

Bello, M. O., Abdus-Salam, N., Adekola, F. A., & Pal, U. (2021). Isotherm and kinetic studies of adsorption of methylene blue using activated carbon from ackee apple pods. *Chemical Data Collections, 31*, 100607. https://doi.org/10.1016/j.cdc.2020.100607

Bhatti, H. N., Safa, Y., Yakout, S. M., Shair, O. H., Iqbal, M., & Nazir, A. (2020). Efficient removal of dyes using carboxymethyl cellulose/alginate/polyvinyl alcohol/rice husk composite: Adsorption/desorption, kinetics and recycling studies. *International Journal of Biological Macromolecules, 150*, 861–870. https://doi.org/10.1016/j.ijbiomac.2020.02.093

Boughrara, L., Zaoui, F., Sebba, F. Z., Bounaceur, B., & Kada, S. O. (2022). New alginic acid derivatives ester for methylene blue dye adsorption: Kinetic, isotherm, thermodynamic, and mechanism study. *International Journal of Biological Macromolecules, 205*, 651–663. https://doi.org/10.1016/j.ijbiomac.2022.02.087

Çatlıoğlu, F., Akay, S., Turunç, E., Gözmen, B., Anastopoulos, I., Kayan, B., & Kalderis, D. (2021). Preparation and application of Fe-modified banana peel in the adsorption of methylene blue: Process optimization using response surface methodology. *Environmental Nanotechnology, Monitoring & Management, 16*, 100517. https://doi.org/10.1016/j.enmm.2021.100517

Chakraborty, J. N. (2010). Dyeing with reactive dye. In *Fundamentals and Practices in Colouration of Textiles* (pp. 57–75). Woodhead Publishing.

Chattopadhyay, D. P. (2011). Chemistry of dyeing. In *Handbook of textile and industrial dyeing* (pp. 150–183). Woodhead Publishing. https://doi.org/10.1533/9780857093974.1.150

Chowdhury, S., Mishra, R., Saha, P., & Kushwaha, P. (2011). Adsorption thermodynamics, kinetics and isosteric heat of adsorption of malachite green onto chemically modified rice husk. *Desalination, 265*(1-3), 159–168. https://doi.org/10.1016/j.desal.2010.07.047

Debnath, S., & Das, R. (2023). Strong adsorption of CV dye by Ni ferrite nanoparticles for waste water purification: Fits well the pseudo second order kinetic and Freundlich isotherm model. *Ceramics International, 49*(10), 16199–16215. https://doi.org/10.1016/j.ceramint.2023.01.218

Demiral, İ., & Şamdan, C. A. (2016). Preparation and characterisation of activated carbon from pumpkin seed shell using H_3PO_4. *Anadolu University Journal of Science and Technology A-Applied Sciences and Engineering, 17*(1), 125–138. https://doi.org/10.18038/btda.64281

Deng, J., Lei, B., He, A., Zhang, X., Ma, L., Li, S., & Zhao, C. (2013). Toward 3D graphene oxide gels based adsorbents for high-efficient water treatment via the promotion of biopolymers. *Journal of Hazardous Materials, 263*, 467–478. https://doi.org/10.1016/j.jhazmat.2013.09.065

Dovi, E., Aryee, A. A., Kani, A. N., Mpatani, F. M., Li, J., Li, Z., et al. (2021). Functionalization of walnut shell by grafting amine groups to enhance the adsorption of Congo red from water in batch and fixed-bed column modes. *Journal of Environmental Chemical Engineering, 9*(5), 106301. https://doi.org/10.1016/j.jece.2021.106301

Ducheyne, P. (2015). *Comprehensive biomaterials*. Elsevier.

El Kassimi, A., Achour, Y., El Himri, M., Laamari, R., & El Haddad, M. (2023). Removal of two cationic dyes from aqueous solutions by adsorption onto local clay: Experimental and theoretical study using DFT method. *International Journal of Environmental Analytical Chemistry, 103*(6), 1223–1244. https://doi.org/10.1080/03067319.2021.1873306

Gad, Y. H., Helal, R. H., Radi, H., El-Nemr, K. F., & Khozemy, E. E. (2023). Preparation and application of irradiated polyvinyl alcohol/starch/pumice composites for adsorption of basic dye: Isotherm and kinetics study. *International Journal of Biological Macromolecules, 249*, 126106. https://doi.org/10.1016/j.ijbiomac.2023.126106

Gaikwad, S. H., & Mukherjee, S. P. (2021). 2D MoO2/N-doped-carbon nanosheets as SERS tweezers: A non-noble metal reusable substrate for selective organic dye detection. *ACS Applied Nano Materials, 4*(11), 11611–11624. https://doi.org/10.1021/acsanm.1c02151

Gandhi, N., Sirisha, D., & Sekhar, K. C. (2016). Adsorption of Fluoride (F-) from aqueous solution by using pineapple (Ananas comosus) peel and orange (Citrus sinensis) peel powders. *International Journal of Environmental Bioremediation & Biodegradation, 4*(2), 55–67. https://doi.org/10.12691/ijebb-4-2-4

Ghibate, R., Senhaji, O., & Taouil, R. (2021). Kinetic and thermodynamic approaches on Rhodamine B adsorption onto pomegranate peel. *Case Studies in Chemical and Environmental Engineering, 3*, 100078. https://doi.org/10.1016/j.cscee.2020.100078

Gong, R., Li, M., Yang, C., Sun, Y., & Chen, J. (2005). Removal of cationic dyes from aqueous solution by adsorption on peanut hull. *Journal of Hazardous Materials, 121*(1-3), 247–250. https://doi.org/10.1016/j.jhazmat.2005.01.029

Gonultas, O., & Candan, Z. (2018). Chemical characterization and ftir spectroscopy of thermally compressed eucalyptus wood panels. *Maderas. Ciencia y tecnología, 20*(3), 431–442. https://doi.org/10.4067/S0718-221X2018005031301

Gopalakrishnan, M., Punitha, V., & Saravanan, D. (2019). Water conservation in textile wet processing. In *Water in*

textiles and fashion (pp. 135–153). Woodhead Publishing. https://doi.org/10.1016/B978-0-08-102633-5.00008-7

Hadjiivanov, K. I., Panayotov, D. A., Mihaylov, M. Y., Ivanova, E. Z., Chakarova, K. K., Andonova, S. M., & Drenchev, N. L. (2020). Power of infrared and Raman spectroscopies to characterize metal-organic frameworks and investigate their interaction with guest molecules. *Chemical Reviews, 121*(3), 1286–1424. https://doi.org/10.1021/acs.chemrev.0c00487

Hameed, B. H., & El-Khaiary, M. I. (2008). Removal of basic dye from aqueous medium using a novel agricultural waste material: Pumpkin seed hull. *Journal of Hazardous Materials, 155*(3), 601–609. https://doi.org/10.1016/j.jhazmat.2007.11.102

Han, W., Li, A., Memon, A., & Ma, M. (2021). Synergetic effect of water, temperature, and pressure on methane adsorption in shale gas reservoirs. *ACS omega, 6*(3), 2215–2229. https://doi.org/10.1021/acsomega.0c05490

Huang, Y., Lee, X., Grattieri, M., Macazo, F. C., Cai, R., & Minteer, S. D. (2018). A sustainable adsorbent for phosphate removal: Modifying multi-walled carbon nanotubes with chitosan. *Journal of Materials Science, 53*(17), 12641–12649. https://doi.org/10.1007/s10853-018-2494-y Internet: https://www.indiamart.com/, Accessed: 28.01.2024

Ip, A. W. M., Barford, J. P., & McKay, G. (2009). Reactive Black dye adsorption/desorption onto different adsorbents: Effect of salt, surface chemistry, pore size and surface area. *Journal of Colloid and Interface Science, 337*(1), 32–38. https://doi.org/10.1016/j.jcis.2009.05.015

Kazemi, M., Navarchian, A. H., & Ahangaran, F. (2023). Effects of silica surface modification with silane and poly (ethylene glycol) on flexural strength, protein-repellent, and antibacterial properties of acrylic dental nanocomposites. *Dental Materials, 39*(10), 863–871. https://doi.org/10.1016/j.dental.2023.07.010

Khumalo, S. M., Bakare, B. F., & Rathilal, S. (2024). Single and multicomponent adsorption of amoxicillin, ciprofloxacin, and sulfamethoxazole on chitosan-carbon nanotubes hydrogel beads from aqueous solutions: Kinetics, isotherms, and thermodynamic parameters. *Journal of Hazardous Materials Advances, 13*, 100404. https://doi.org/10.1016/j.hazadv.2024.100404

Kowalkowska, A., & Jóźwiak, T. (2019). Utilization of pumpkin (Cucurbita pepo) seed husks as a low-cost sorbent for removing anionic and cationic dyes from aqueous solutions. *Desalination and Water Treatment, 171*, 397–407. https://doi.org/10.5004/dwt.2019.24761

Kumar, P. S., Ramalingam, S., Senthamarai, C., Niranjanaa, M., Vijayalakshmi, P., & Sivanesan, S. (2010). Adsorption of dye from aqueous solution by cashew nut shell: Studies on equilibrium isotherm, kinetics and thermodynamics of interactions. *Desalination, 261*(1-2), 52–60. https://doi.org/10.1016/j.desal.2010.05.032

Li, D., Gao, Z., Zhang, B., Ma, W., Tang, B., & Zhang, S. (2024). Excellent fixation of low-water-soluble reactive dyes containing vinylsulfone group for nylon dyeing. *Dyes and Pigments, 222*, 111887. https://doi.org/10.1016/j.dyepig.2023.111887

Li, Q., Yue, Q. Y., Su, Y., Gao, B. Y., & Li, J. (2009). Two-step kinetic study on the adsorption and desorption of reactive dyes at cationic polymer/bentonite. *Journal of Hazardous Materials, 165*(1-3), 1170–1178. https://doi.org/10.1016/j.jhazmat.2008.10.110

Mahmoodi, N. M., Arami, M., Bahrami, H., & Khorramfar, S. (2010). Novel biosorbent (Canola hull): Surface characterization and dye removal ability at different cationic dye concentrations. *Desalination, 264*(1-2), 134–142. https://doi.org/10.1016/j.desal.2010.07.017

Martini, B. K., Daniel, T. G., Corazza, M. Z., & de Carvalho, A. E. (2018). Methyl orange and tartrazine yellow adsorption on activated carbon prepared from boiler residue: Kinetics, isotherms, thermodynamics studies and material characterization. *Journal of Environmental Chemical Engineering, 6*(5), 6669–6679. https://doi.org/10.1016/j.jece.2018.10.013

Meskel, A. G., Kwikima, M. M., Meshesha, B. T., Habtu, N. G., Naik, S. C. S., & Vellanki, B. P. (2024). Malachite green and methylene blue dye removal using modified bagasse fly ash: Adsorption optimization studies. *Environmental Challenges, 14*, 100829. https://doi.org/10.1016/j.envc.2023.100829

Mihaylov, M., Lagunov, O., Ivanova, E., & Hadjiivanov, K. (2011). Determination of polycarbonyl species on nickel-containing catalysts by adsorption of CO isotopic mixtures. *Topics in Catalysis, 54*, 308–317. https://doi.org/10.1007/s11244-011-9661-6

Miyah, Y., Lahrichi, A., Idrissi, M., Khalil, A., & Zerrouq, F. (2018). Adsorption of methylene blue dye from aqueous solutions onto walnut shells powder: Equilibrium and kinetic studies. *Surfaces and Interfaces, 11*, 74–81. https://doi.org/10.1016/j.surfin.2018.03.006

Moradzaman, M., & Mul, G. (2020). Infrared analysis of interfacial phenomena during electrochemical reduction of CO2 over polycrystalline copper electrodes. *ACS Catalysis, 10*(15), 8049–8057. https://doi.org/10.1021/acscatal.0c02130

Müller, V., Piai, J. F., Fajardo, A. R., Fávaro, S. L., Rubira, A. F., & Muniz, E. C. (2011). Preparation and characterization of zein and zein-chitosan microspheres with great prospective of application in controlled drug release. *Journal of Nanomaterials, 2011*, 1–6. https://doi.org/10.1155/2011/928728

Okoye, A. I., Ejikeme, P. M., & Onukwuli, O. D. (2010). Lead removal from wastewater using fluted pumpkin seed shell activated carbon: Adsorption modeling and kinetics. *International Journal of Environmental Science & Technology, 7*(4), 793–800. https://doi.org/10.1007/BF03326188

Pazo-Cepeda, M. V., Nastasiienko, N. S., Kulik, T. V., Palianytsia, B. B., Alonso, E., & Aspromonte, S. G. (2023). Adsorption and thermal transformation of lignin model compound (ferulic acid) over HY zeolite surface studied by temperature programmed desorption mass-spectrometry, FTIR and UV–Vis spectroscopy. *Microporous and Mesoporous Materials, 348*, 112394. https://doi.org/10.1016/j.micromeso.2022.112394

Pepper, I. L. (2019). Biotic characteristics of the environment. In *Environmental and Pollution Science* (pp. 61–87). Academic Press. https://doi.org/10.1016/B978-0-12-814719-1.00005-7

Purkait, M. K., DasGupta, S., & De, S. (2005). Adsorption of eosin dye on activated carbon and its surfactant based

desorption. *Journal of Environmental Management, 76*(2), 135–142. https://doi.org/10.1016/j.jenvman.2005.01.012

Qin, S., Wang, J., Zhao, C., & Zhang, S. (2010). Long-term, low temperature simulation of early diagenetic alterations of organic matter: A FTIR study. *Energy Exploration & Exploitation, 28*(5), 365–376. https://doi.org/10.1260/0144-5987.28.5.365

Rashid, J., Tehreem, F., Rehman, A., & Kumar, R. (2019). Synthesis using natural functionalization of activated carbon from pumpkin peels for decolourization of aqueous methylene blue. *Science of the Total Environment, 671*, 369–376. https://doi.org/10.1016/j.scitotenv.2019.03.363

Rawat, S., & Ahammed, M. M. (2023). Dye removal by clay-pumpkin seed cake composite: modelling and optimization. *International Journal of Environmental Science and Technology, 20*(11), 12481–12498. https://doi.org/10.1007/s13762-022-04667-x

Roy, M., & Saha, R. (2021). Dyes and their removal technologies from wastewater: A critical review. *Intelligent Environmental Data Monitoring for Pollution Management*, 127–160. https://doi.org/10.1016/B978-0-12-819671-7.00006-3

Sadoq, M., Atlas, H., Imame, S., Kali, A., Amar, A., Loulidi, I., et al. (2024). Elimination of crystal violet from aqueous solution by adsorption on naturel polysaccharide: Kinetic, isotherm, thermodynamic studies and mechanism analysis. *Arabian Journal of Chemistry, 17*(1), 105453. https://doi.org/10.1016/j.arabjc.2023.105453

Schramm, C. (2020). High temperature ATR-FTIR characterization of the interaction of polycarboxylic acids and organotrialkoxysilanes with cellulosic material. *Spectrochimica Acta Part A: Molecular and Biomolecular Spectroscopy, 243*, 118815. https://doi.org/10.1016/j.saa.2020.118815

Senthilkumaar, S., Kalaamani, P., Porkodi, K., Varadarajan, P. R., & Subburaam, C. V. (2006). Adsorption of dissolved reactive red dye from aqueous phase onto activated carbon prepared from agricultural waste. *Bioresource Technology, 97*(14), 1618–1625. https://doi.org/10.1016/j.biortech.2005.08.001

Shunda, I., Lu, Y., Zheng, L., Long, L., Jiang, X., & Yan, J. (2023). Mechanism study of Cu (II) adsorption from acidic wastewater by ultrasonic-modified municipal solid waste incineration fly ash. *Chinese Journal of Chemical Engineering*. https://doi.org/10.1016/j.cjche.2023.11.019

Singh, V. K., Sett, A., & Karmakar, S. (2024). Waste to wealth: Facile activation of red mud waste and insights into industrial reactive dye removal from wastewater. *Chemical Engineering Journal, 481*, 148373. https://doi.org/10.1016/j.cej.2023.148373

Siraorarnroj, S., Kaewtrakulchai, N., Fuji, M., & Eiad-ua, A. (2022). High performance nanoporous carbon from mulberry leaves (Morus alba L.) residues via microwave treatment assisted hydrothermal-carbonization for methyl orange adsorption: Kinetic, equilibrium and thermodynamic studies. *Materialia, 21*, 101288. https://doi.org/10.1016/j.mtla.2021.101288

Stavrinou, A., Aggelopoulos, C. A., & Tsakiroglou, C. D. (2018). Exploring the adsorption mechanisms of cationic and anionic dyes onto agricultural waste peels of banana, cucumber and potato: Adsorption kinetics and equilibrium isotherms as a tool. *Journal of Environmental Chemical Engineering, 6*(6), 6958–6970. https://doi.org/10.1016/j.jece.2018.10.063

Strauss, I., Chakarova, K., Mundstock, A., Mihaylov, M., Hadjiivanov, K., Guschanski, N., & Caro, J. (2020). UiO-66 and UiO-66-NH2 based sensors: Dielectric and FTIR investigations on the effect of CO2 adsorption. *Microporous and Mesoporous Materials, 302*, 110227. https://doi.org/10.1016/j.micromeso.2020.110227

Subbaiah, M. V., & Kim, D. S. (2016). Adsorption of methyl orange from aqueous solution by aminated pumpkin seed powder: Kinetics, isotherms, and thermodynamic studies. *Ecotoxicology and Environmental Safety, 128*, 109–117. https://doi.org/10.1016/j.ecoenv.2016.02.016

Sulak, M. T., Demirbas, E., & Kobya, M. (2007). Removal of Astrazon Yellow 7GL from aqueous solutions by adsorption onto wheat bran. *Bioresource Technology, 98*(13), 2590–2598. https://doi.org/10.1016/j.biortech.2006.09.010

Sultana, S., Islam, K., Hasan, M. A., Khan, H. J., Khan, M. A. R., Deb, A., et al. (2022). Adsorption of crystal violet dye by coconut husk powder: Isotherm, kinetics and thermodynamics perspectives. *Environmental Nanotechnology, Monitoring & Management, 17*, 100651. https://doi.org/10.1016/j.enmm.2022.100651

Taqui, S. N., Syed, A. A., Mubarak, N. M., Farade, R. A., Khan, M. M., Kalam, M. A., et al. (2023). Insights into isotherms, kinetics, and thermodynamics of adsorption of acid blue 113 from an aqueous solution of nutraceutical industrial fennel seed spent. *Scientific Reports, 13*(1), 22665. https://doi.org/10.1038/s41598-023-49471-w

Vunain, E., Kenneth, D., & Biswick, T. (2017). Synthesis and characterization of low-cost activated carbon prepared from Malawian baobab fruit shells by H 3 PO 4 activation for removal of Cu (II) ions: Equilibrium and kinetics studies. *Applied Water Science, 7*, 4301–4319. https://doi.org/10.1007/s13201-017-0573-x

Wang, S., Vakili, M., Guan, T., Zhu, X., Zhou, S., Wang, W., & Gong, W. (2024). Adsorption of typical dyes in water by sponge based covalent organic frameworks: Pore size and mechanism. *Colloids and Surfaces A: Physicochemical and Engineering Aspects, 685*, 133312. https://doi.org/10.1016/j.colsurfa.2024.133312

Wang, Y., Saad, A. M., Saur, O., Lavalley, J. C., & Morrow, B. A. (1998). FTIR study of adsorption and reaction of SO2 and H2S on Na/SiO2. *Applied Catalysis B: Environmental, 16*(3), 279–290. https://doi.org/10.1016/S0926-3373(97)00084-2

Wasewar, K. L., Singh, S., & Kansal, S. K. (2020). Process intensification of treatment of inorganic water pollutants. In *Inorganic Pollutants in Water* (pp. 245–271). Elsevier. https://doi.org/10.1016/B978-0-12-818965-8.00013-5

Wen, P., Gong, P., Mi, Y., Wang, J., & Yang, S. (2014). Scalable fabrication of high quality graphene by exfoliation of edge sulfonated graphite for supercapacitor application. *RSC Advances, 4*(68), 35914–35918. https://doi.org/10.1039/C4RA04788E

Witek-Krowiak, A., Szafran, R. G., & Modelski, S. (2011). Biosorption of heavy metals from aqueous solutions onto peanut shell as a low-cost biosorbent. *Desalination,*

265(1-3), 126–134. https://doi.org/10.1016/j.desal.2010.07.042

Xu, X., Liu, H., Duan, S., Liu, X., Zhang, K., & Tu, J. (2020). A novel pumpkin seeds protein-pea starch edible film: Mechanical, moisture distribution, surface hydrophobicity, UV-barrier properties and potential application. *Materials Research Express, 6*(12), 125355. https://doi.org/10.1088/2053-1591/ab63f7

Yin, H., Xiong, Q., Zhang, M., Wang, B., & Zhang, F. (2023). Multi-principles analysis of Cu (II) adsorption in water on magnetic microspheres and modified chitosan. *Journal of Environmental Chemical Engineering, 11*(6), 111285. https://doi.org/10.1016/j.jece.2023.111285

Yu, B., Zhang, Y., Shukla, A., Shukla, S. S., & Dorris, K. L. (2000). The removal of heavy metal from aqueous solutions by sawdust adsorption—removal of copper. *Journal of Hazardous Materials, 80*(1-3), 33–42. https://doi.org/10.1016/S0304-3894(00)00278-8

Zhang, B., Gao, B., Ma, W., Mo, Z., Song, Y., Xie, S., et al. (2023). Adsorption of uranium (VI) by natural vermiculite: Isotherms, kinetic, thermodynamic and mechanism studies. *Journal of Environmental Radioactivity, 270*, 107305. https://doi.org/10.1016/j.jenvrad.2023.107305

Zhao, B., Xiao, W., Shang, Y., Zhu, H., & Han, R. (2017). Adsorption of light green anionic dye using cationic surfactant-modified peanut husk in batch mode. *Arabian Journal of Chemistry, 10*, S3595–S3602. https://doi.org/10.1016/j.arabjc.2014.03.010

Zimmerman, D. A., Koenig, J. L., & Ishida, H. (1999). Infrared and Raman spectroscopy of cyclohexa (p-phenylene sulfide) and the polymer obtained therefrom. *Polymer, 40*(17), 4723–4731. https://doi.org/10.1016/S0032-3861(98)00635-1